Electronic Supplementary Material (ESI) for Nanoscale.

Supporting Information

Nitrogen and fluorine dual-doped mesoporous graphene: high-performance metal-free ORR electrocatalyst with superlow HO_2^- yield

Shu Jiang,[a,b] Yujing Sun,[a] Haichao Dai,[a,b] Jingting Hu,[a,b] Pengjuan Ni,[a,b] Yilin Wang,[a,b] Zhen Li,[a,b] Zhuang Li[a, *]

[a]State Key Laboratory of Electroanalytical Chemistry, Changchun Institute of Applied Chemistry, Chinese Academy of Sciences, Changchun, Jilin 130022, People's Republic of China

[b]University of Chinese Academy of Sciences, Beijing 100049, People's Republic of China

* Corresponding author. Tel./Fax: +86 431 85262057.
E-mail address: zli@ciac.ac.cn

1. Experimental Section

1.1 Chemicals

Graphite and commercial carbon-supported Pt catalyst (20 wt%, Pt/C) were purchased from Alfa Aesar. Ammonium peroxydisulfate ($(NH_4)_2S_2O_8$) was purchased from Xilong Chemical Industry Co. Ltd. (Guangdong, China). Concentrated sulfuric acid (H_2SO_4) and ammonium fluoride (NH_4F) were obtained from Beijing Chemical Factory (Beijing, China). Unless otherwise stated, other reagents were of analytical grade and were used without further purification. All aqueous solutions were prepared with ultrapure water (>18 MΩ) from an automatic double distillation system (Shanghai, China).

1.2 Apparatus

A XL30 ESEM scanning electron microscope (SEM) was used to determine the morphology. Transmission electron microscopy (TEM) measurements were made on a HITACHI H-8100 EM with an accelerating voltage of 100 kV. High-resolution TEM (HRTEM) images were obtained with a TECNAI G2 high-resolution transmission electron microscope operating at 200 kV. X-Ray diffraction (XRD) patterns were obtained using a D8 ADVANCE (Bruker AXS, Germany) using Cu Kα (1.5406 Å) radiation. X-Ray photoelectron spectroscopy (XPS) analysis was carried on an ESCALAB-MK II 250 photoelectron spectrometer (VG Scientifc, UK) with Al Kα X-ray radiation as the X-ray source for excitation. Electrochemical measurements were performed with a CHI 832C electrochemical analyzer (CH Instruments, Inc., USA). A conventional three-electrode cell was used, including an Ag/AgCl (sat. KCl) electrode as the reference electrode, a platinum wire as the counter electrode and rotating ring disk electrode (RRDE, 4 mm in disk diameter) as the working electrode. RRDE tests were conducted on RRDE-3A apparatus (ALS Company, Japan) with the Glassy Carbon disk and Pt ring electrode and the CHI 832C electrochemical analyzer. The electrochemical impedance (EIS) experiments were performed by Autolab with PGSTAT 30 (Eco Chemie B.V., Utrecht, Netherlands) and with the aid of frequency response analysis system software under an oscillation potential of 5 mV over a frequency range of 100 kHz to 0.01

Hz. Nitrogen adsorption-desorption isotherms were measured with a Quadrachrome Autosorb Automated Gas Sorption System. The pore size distribution was determined via the Barrett-Joyner-Halenda formula (BJH) method using nitrogen adsorption data. The specific surface area was calculated using the BET equation. The Raman spectroscopy was performed using a Renishaw 2000 model confocal microscopy Raman spectrometer with a CCD detector and a holographic notch filter (Renishaw Ltd., Gloucestershire, UK) with a wavelength of 514.5 nm produced by an air-cooled argon ion laser.

1.3 Synthesis of graphene oxide (GO)

The graphite oxide was synthesized from natural graphite powder according to Hummer method with minor modification.[1] Then, exfoliation of graphite oxide was performed by ultrasonication of the dispersion for more than 30 min. Finally, a homogeneous GO aqueous dispersion (2 mg mL^{-1}) was obtained for further use.

1.4 *In situ* synthesis of GO/PANI composites

First, 10 mL GO (2 mg mL^{-1}) was mixed with 300 μL aniline (Ani) dispersed in 10 mL H_2SO_4 (1M)) under stirring to form a uniform solution. Then, 30 mL $(NH_4)_2S_2O_8$ (750 mg) solution was added dropwise into the above solution. The mixed solution was vigorously stirred for 24 h at 0~5 °C to obtain graphene oxide/polyaniline (GO/PANI) composite.

1.5 Synthesis of NF-MG nanosheets

In a typical synthesis, a given amount of the obtained GO/PANI powder and NH_4F were firstly dispersed in 10 mL H_2O. The mixture was stirred for about 2 h and dried overnight at 60 ˚C. Then the ground resulting powder was pyrolysed at 400 ˚C for 30 min, 900 ˚C for 1 h under a continuous flow of argon atmosphere. After that, the sample was cooled down to room temperature and collected from the quartz tube. The pyrolysed product was ground with a mortar and pestle and denoted as NF-MG. For comparison, F-G and F-PANI were prepared in a similar way as described above within the mass ratio of NH_4F to GO or PANI being 30. In this work, the mass ratio of NH_4F and GO/PANI was set to be 10, 20, 30, 40 to investigate the effect of different F content on ORR performance. As a result, the F doped samples were denoted as NF-MG1, NF-MG2, NF-MG3 and NF-MG4, respectively. At the same time, GO, PANI and GO/PANI were also pyrolysed under the same condition with or without the addition of Ani or NH_4F in the first step, for simplicity, which were denoted as G, PANI and N-G, respectively. For simplicity, the preparation of NF-MG is illustrated as below.

Scheme 1 illustration of NF-MG preparation.

1.6 Electrocatalytic activity evaluation

The activity for ORR was evaluated by voltamperometry by the N and

F-codoped G as electrodes. Fabrication of the working electrodes was done by pasting catalyst inks on a RRDE electrode. The carbon ink was formed by mixing 5 mg of nitrogen F-doped G catalysts, 800 μL of water, 190 μL of isopropyl alcohol, and 10 μL of 5 wt % Nafion in a plastic vial under ultra-sonication. A 10-μL aliquot of the carbon ink was dropped on the surface of the glassy carbon rotating disk electrode, yielding an approximate catalyst loading of 0.40 mg cm^{-2}. For comparison, a commercially available platinum/carbon catalyst, nominally 20 wt % on carbon black from E-TEK was used. The platinum based ink was obtained in the same way, yielding an approximate mass loading of 80 μg_{Pt} cm^{-2}. To remove the capacitive current of the working electrode, the background current was measured by running the above electrodes in N_2-purged KOH electrolyte before the ORR measurements and subtracted from the ORR polarization curve. Therefore, the net faradic current of ORR was obtained for evaluation of the ORR activity. Cyclic voltammogram (CV) was performed from 1.147 to -0.053 V at 50 mV s^{-1} after purging the electrolyte with O_2 or N_2 gas for 30 min. Linear sweep voltammogram (LSV) measurements were performed by using the rotating disk electrode (RDE) at different rotating speed from 400 to 2500 rpm in an O_2-saturated electrolyte from 1.147 to -0.053 V at a sweep rate of 10 mV s^{-1} for our as-prepared samples. The LSV polarization for Pt/C was measured from -0.053 to 1.147 V in order to remove the side effect of anions adsorption on Pt.[2] Koutecky-Levich (K-L) equation was used for analyzing the transferred electron number (n) during the ORR with disk currents.[3, 4]

$$\frac{1}{j}=\frac{1}{j_k}+\frac{1}{j_L}=\frac{1}{B\omega^{1/2}}+\frac{1}{j_L} \qquad (1)$$

$$B=0.62\,nFC_o(D_o)^{2/3}\nu^{-1/6} \qquad (2)$$

$$j_k= nF\kappa C_o \qquad (3)$$

Where j is the overall current density, j_L is the diffusion-limiting current density, j_k is the kinetic current density, ω is the angular velocity of the disk (ω=2πN, N is the linear rotation speed), F is the Faraday constant (96485 C mol^{-1}), C_O is the bulk concentration of O_2 (1.2×10^{-6} mol cm^{-3}), D_O is the diffusion coefficient of O_2 (1.9×10^{-5} cm^2 s^{-1}), ν is the kinematics viscosity of the electrolyte (0.01 cm^2 s^{-1}). For calculation of yields of HO_2^- on different catalysts, based on both ring and disk currents from RRDE, the percentage of HO_2^- generated from ORR in alkaline medium and the electron transfer number (n) were estimated by the following equations:[5, 6]

$$\%\,HO_2^- = 200\times\frac{j_R/N}{j_D+j_R/N}$$

(4)

$$n=4\times\frac{j_D}{j_D+j_R/N}$$

(5)

Where j_D is the disk current density, j_R is the ring current density and N is the current collection efficiency of the Pt ring. N is 0.42 obtained from the reduction of $K_3Fe(CN)_6$. The ring potential of Pt ring is constant at 1.447 V. All the current densities have already been normalized to the electrode surface area (0.1256 cm^2). All potentials were conducted with respect to the reversible hydrogen electrode (RHE). The RHE calibration was done as described in the literature.[7] In detail, we used Ag/AgCl (sat.KCl) as the reference electrode in all measurements. It was calibrated with respect to RHE. The calibration was performed in the high purity hydrogen saturated 0.1 M KOH with a Pt wire as the working electrode. CV was run at a scan rate of 1mV s^{-1}, and the average of the two potentials at which the current crossed zero was taken to be the thermodynamic potential for the hydrogen electrode reactions. The obtained CV was given as below.

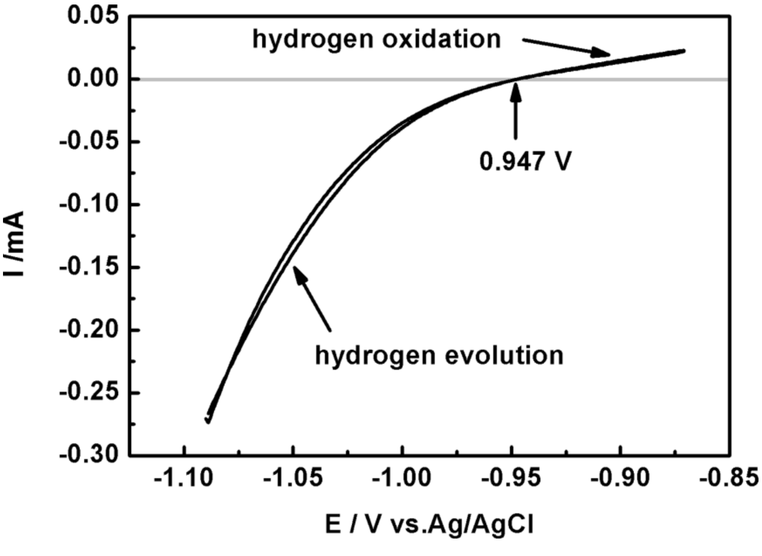

So in 0.1 M KOH, E (RHE) = E (Ag/AgCl (sat.KCl)) + 0.947 V.

2. Optimization and morphology of NF-MGs catalysts

Inspired by Sun’s work on F-doped carbon black as an outstanding metal-free ORR catalyst in alkaline solution,[6] we successfully fabricated a family of N and F co-doped mesoporous G-based electrocatalysts (NF-MGs) for ORR in alkaline medium. By varying the initial mass ratio between NH_4F and GO/PANI in the order of 10 (NF-MG1), 20 (NF-MG2) , 30 (NF-MG3) and 40 (NF-MG4) to decide the optimal F content, then the ORR electrocatalytic activities of NF-MG catalysts were evaluated by LSV in O_2-saturated 0.1 M KOH on a RRDE (Fig. S1). From LSVs (Fig.S1A), we can tell clearly the slight effect of F doping on the catalytic activity of graphene on onset potential (E_{onset}) but distinct influence on half-wave potential ($E_{1/2}$) and diffusion-limiting current (j_L) on the F content. All these three key parameters (E_{onset}, $E_{1/2}$ and j_L) coincidently show the catalytic activity of NF-MG increases first with the F content, then reaches a maximum at an optimal F content (49.7 wt % for NF-MG3, initial weight ratio), and finally decreases at higher F content (50.1 wt % for NF-MG4，initial weight ratio). Interestingly, these four volcano shapes are coincident with the F content dependence of the morphology of these catalysts, as shown in Fig. S2, indicating the more mesopores there are, the better the ORR performance of NF-MG catalyst is. Besides, from RRDE measurements, the lowest amount of HO_2^- generated in ORR for NF-MG3 (Fig.S1B). The N and F doping level were estimated by

XPS spectra. Besides, the surface area and average pore size for NF-MGs were calculated by BET and BJH methods, respectively. The element composition (C, O, N, F) for NF-MGs together with surface area and average pore size were summarized in Table S1. The highest N and F doping level as well as the largest surface area and smallest pore size can be obtained in NF-MG3, which is beneficial to enhance ORR performance. The volcano-shaped dependence of sheet-like morphology on the F content probably is due to the etching of some mesopores and the formation of some macropores at high NH_4F content (Table S1). At an optimal F-content on G-based carbon, the highest performance could be obtained.

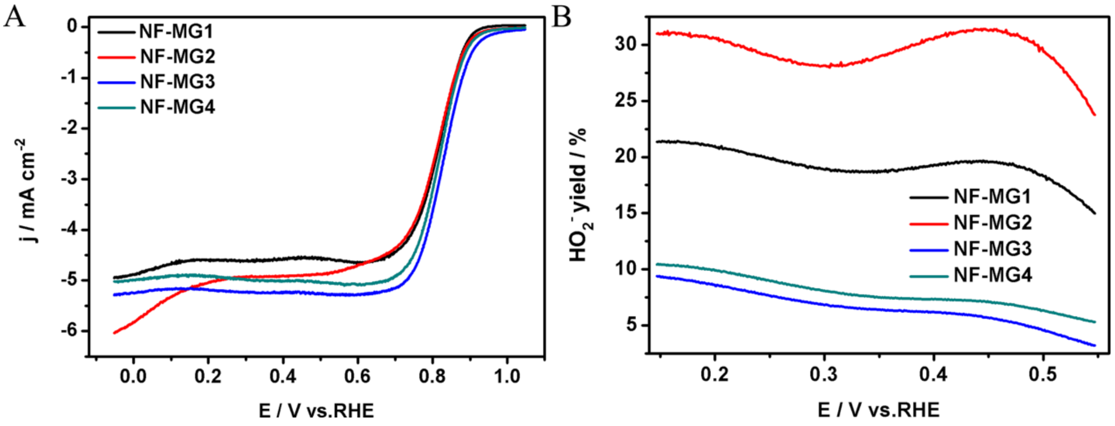

Fig. S1 LSV curves (A) and HO_2^- yield (B) of NF-MG1, NF-MG2, NF-MG3 and NF-MG4 catalysts in O_2-saturated 0.1 M KOH with the scan rate of 10 mV/s and the rotation speed of 1600 rpm.

Table S1 Elemental composition and physicochemical properties of all samples obtained from XPS spectra and N_2 adsorption/desorption analysis

Samples	C (at%)	O (at%)	N (at%)	F (at%)	SA[a] (m^2 g^{-1})	PD[b] (nm)
NF-MG1	86.97	11.36	1.66	0.01	184.9	18.28
NF-MG2	82.43	16.25	1.20	0.12	125.8	31.90
NF-MG3	84.03	13.88	1.96	0.13	131.0	5.66
NF-MG4	82.70	16.00	1.19	0.11	26.32	64.87
F-PANI	88.28	7.79	2.75	1.19	-	-
F-G	82.15	14.82	2.12	0.92	-	-
PANI	80.38	19.32	0.30	-	-	-
N-G	86.09	11.59	2.32	-	-	-

[a] Specific surface area from multiple BET methods. [b] Average pore diameter, estimated using the adsorption branch of the isotherm and the Barrett-Joyner-Halenda formula.

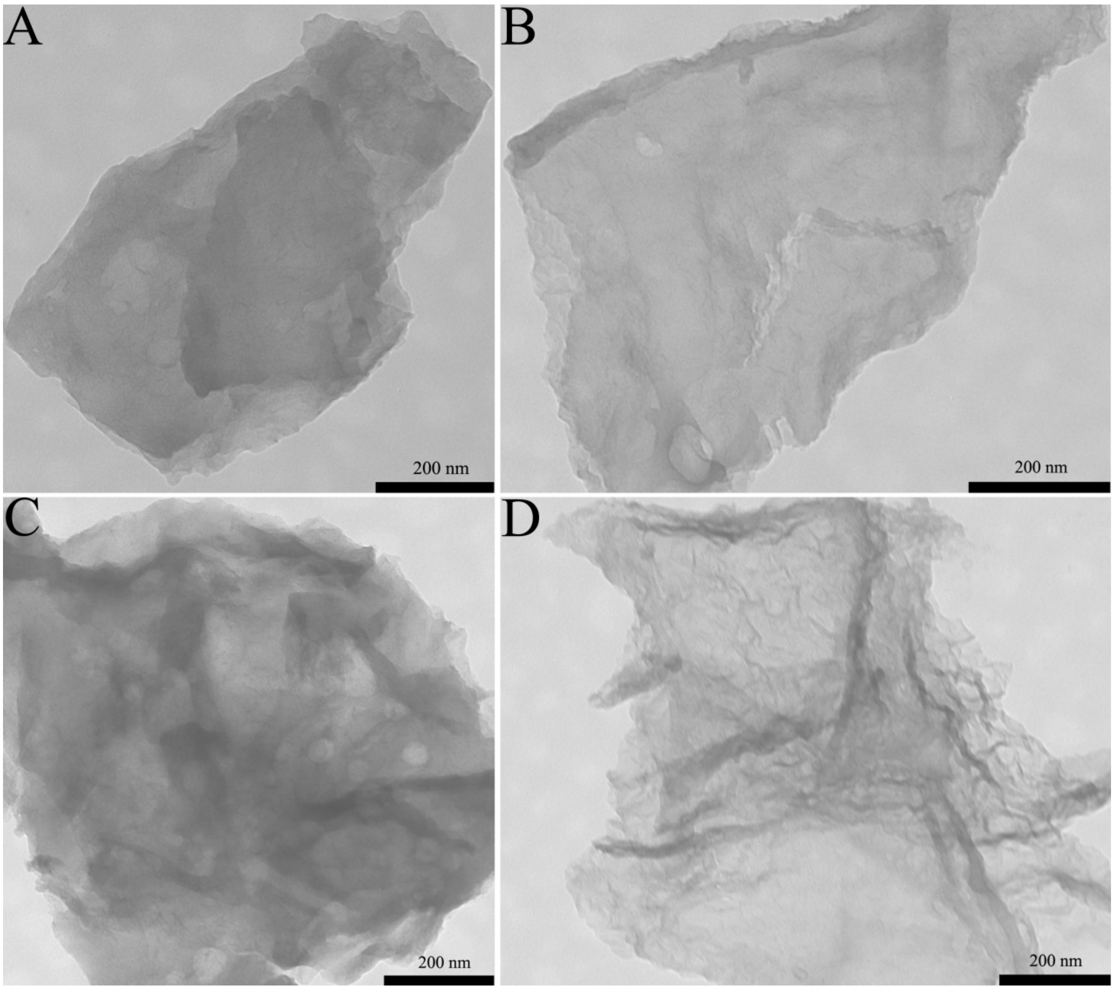

Fig. S2 TEM images of NF-MG1(A), NF-MG2(B), NF-MG3(C), NF-MG4(D).

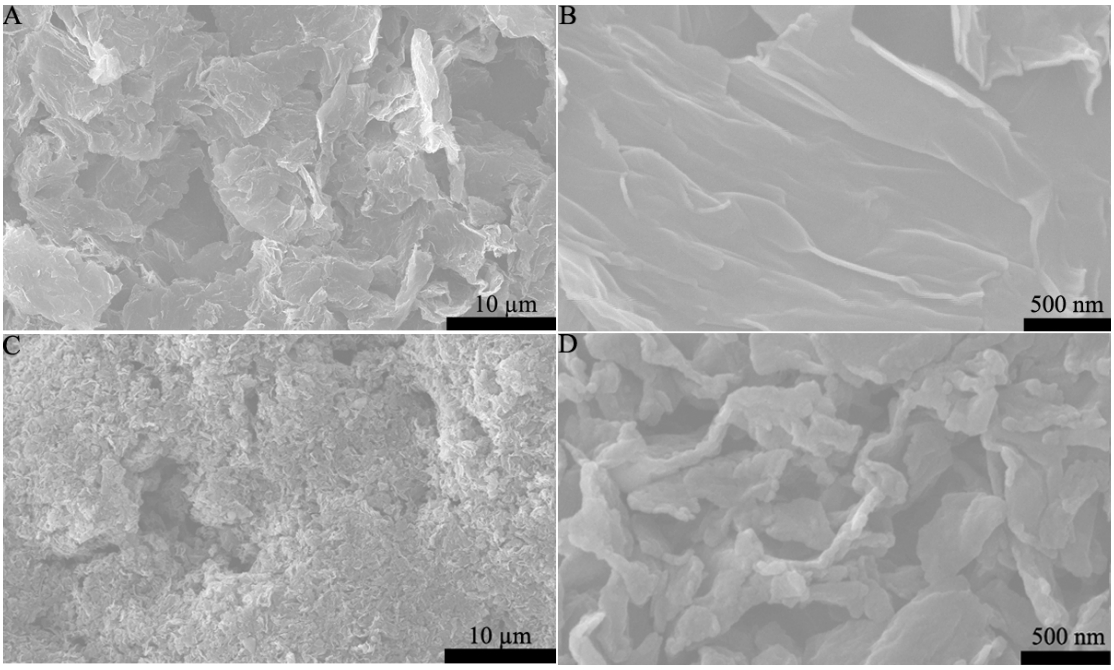

Fig. S3 Low and high magnification SEM images of G (A, B) and NF-MG3(C, D).

3. N and F co-doping influence on morphology and structure of NF-MG3

As shown in Fig. S4A, PANI was demonstrated a structure of sphere-like particles with an average diameter of 50 nm. However, when mixed with NH_4F to synthesize F-PANI under high temperature, the sphere-like particle turned into sheet-like cube (Fig. S4C). Besides, much thinner sheet with a similar shape like G was formed for F doped G denoted as F-G (Fig. S4B), whereas much thicker sheet exhibit on the surface of N doped G designated as N-G (Fig. S4D). Such a distinct difference on the morphology of as-prepared samples should have a great effect on their ORR activity which was discussed in detail in the plain text.

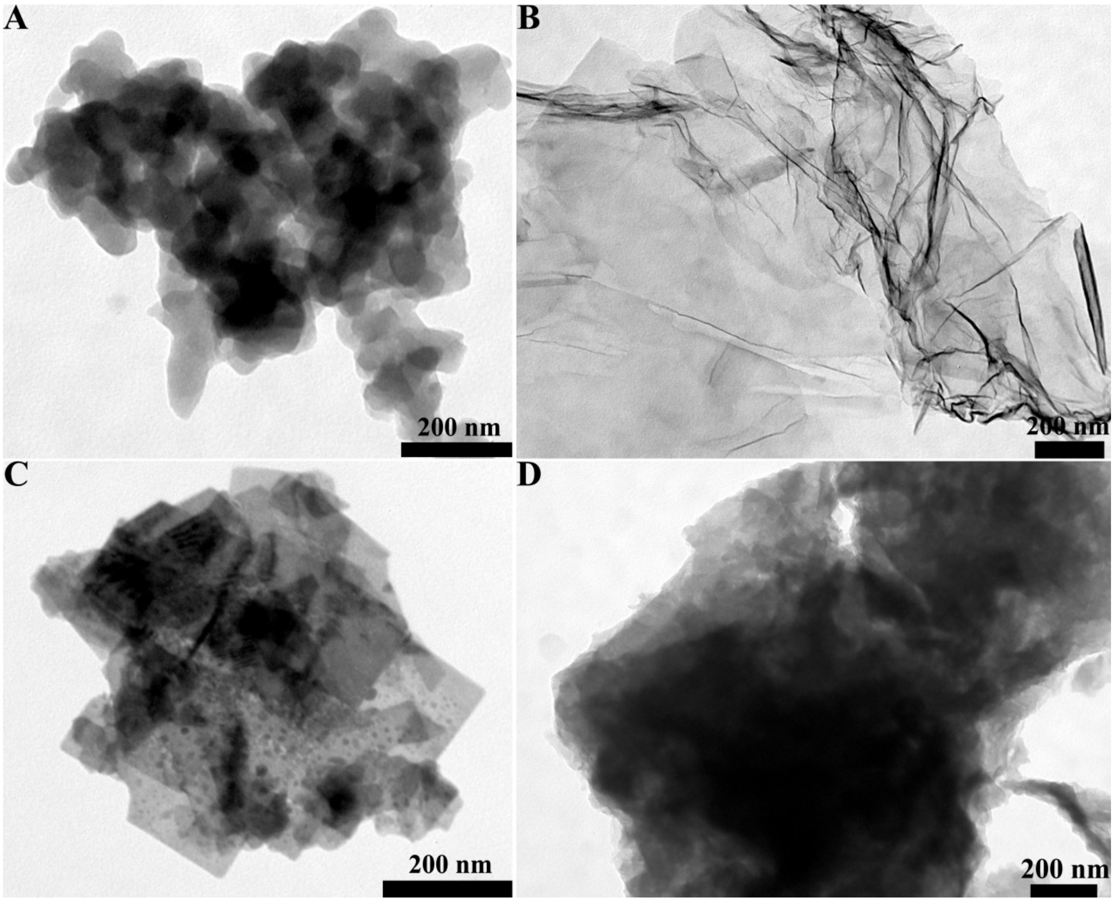

Fig. S4 TEM images of PANI(A), F-G(B), F-PANI(C), N-G(D).

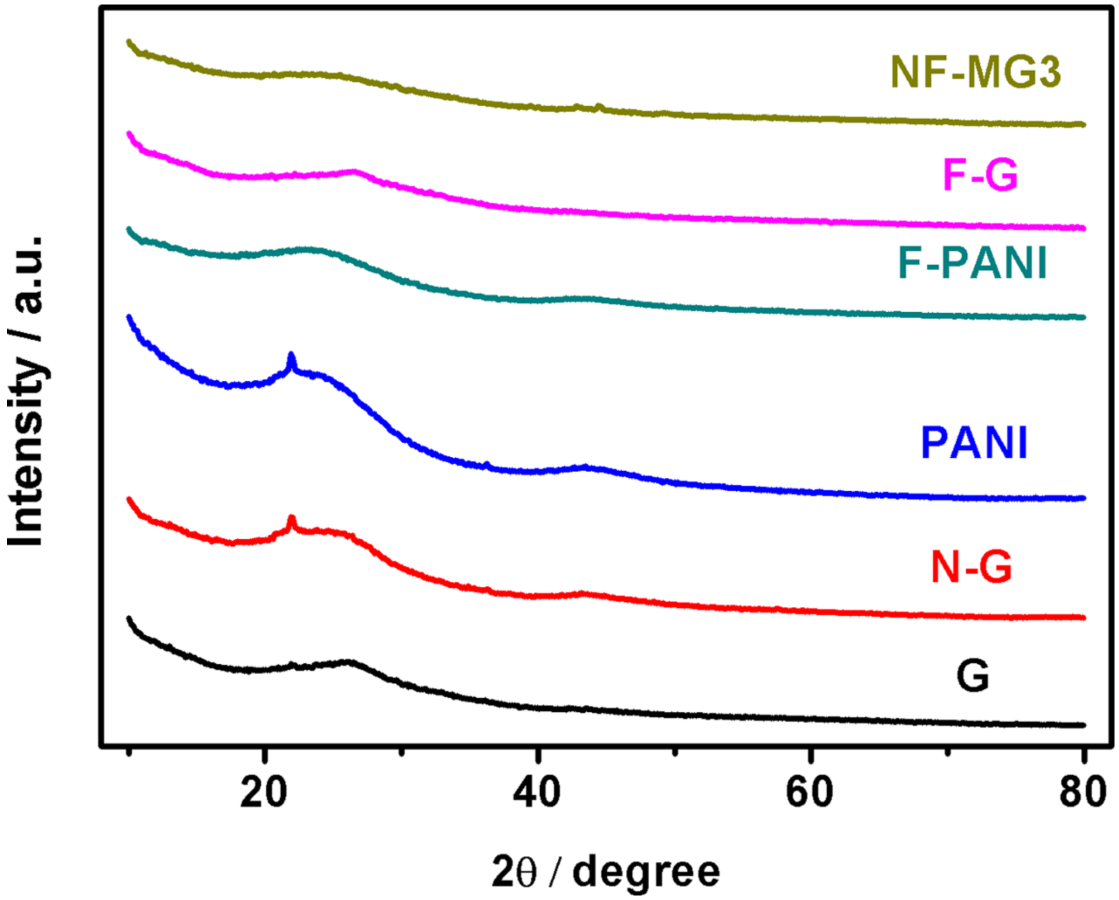

Fig. S5 XRD patterns of G, N-G, PANI, F-PANI, F-G and NF-MG3.

The structure of the as-prepared samples were investigated by X-ray diffraction (XRD) (Fig. S5). The XRD pattern clearly confirmed the successful reduction of the GO and formation of graphitic structures. Generally, a sharp peak at 11.5° corresponding to the (001) reflection, which is a characteristic peak of GO,[8, 9] disappeared for all G-based samples upon thermal treatment. Following the heat treatment, a broad peak located at approximately 26° which can be attributed to the characteristic (002) lattice plane of the G sheets reappeared in the spectrum for the G-based samples.[10] The diffraction peaks at 2θ around 42.2 and 44.3°

correspond to the (100) and (101) reflections of G sheets respectively.[11] Interestingly, similar peaks also appeared in PANI and F-PANI which indicated their graphic framework formed. However, after F doping in PANI, G and NF-MG3 via pyrolysis, the peak located at 26° becomes broader suggesting more amorphous carbon formed under the same condition.

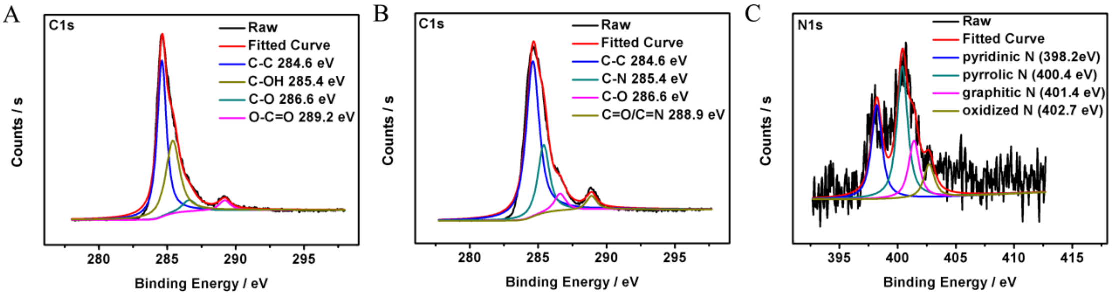

Fig. S6 High-resolution XPS spectrum of C 1s and N 1s of G (A), N-G (B, C).

4. N and F co-doping influence on ORR activity of NF-MG3

Table S2 Electrochemical parameters for ORR estimated from CVs and RDE polarization curves in 0.1 M KOH solution

Electrocatalysts	E_{peak}^a (V)	j_{peak}^a (mA cm^{-2})	E_{onset}^b (V)	$E_{1/2}^b$ (V)	j^b (mA cm^{-2}) at 0.3 V
G	0.565	-0.534	0.734	0.603	-1.293
PANI	0.695	-0.814	0.826	0.669	-3.017
N-G	0.704	-0.972	0.818	0.709	-2.899
F-PANI	0.760	-1.746	0.903	0.770	-4.243
F-G	0.765	-2.032	0.965	0.820	-4.893
NF-MG3	0.776	-4.911	1.047	0.828	-5.234
Pt/C	0.812	-2.832	1.041	0.860	-5.387

[a] obtained from Fig. 5A [b] obtained from Fig. 5B

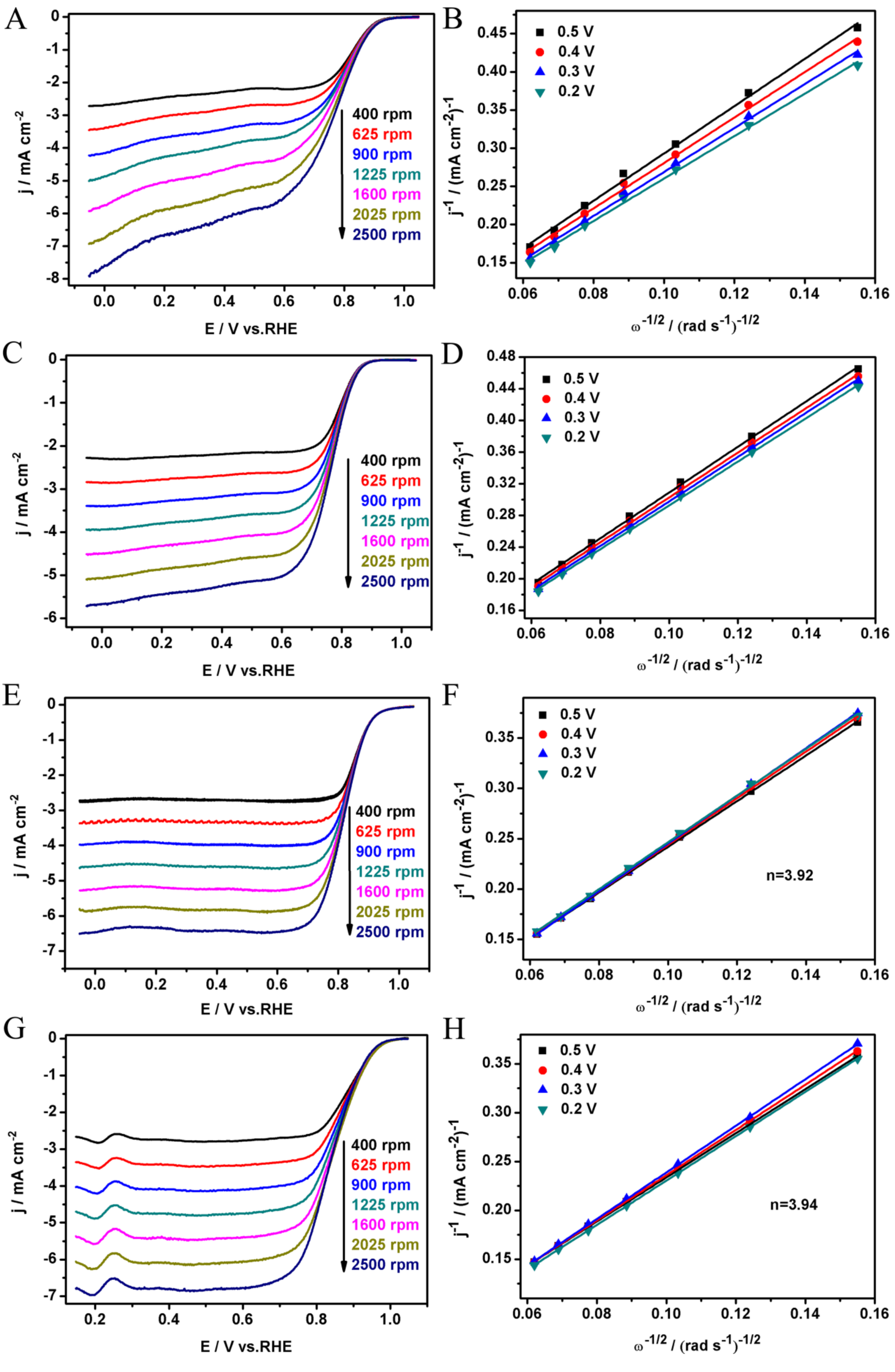

Fig. S7 RDE voltammograms of F-G (A), F-PANI (C), NF-MG3 (E) and Pt/C (G) in O_2-saturated 0.1 M KOH with various rotation rates at a scan rate of 10 mV s^{-1}. K-L plots of F-G (B), F-PANI (D), NF-MG3 (F) and Pt/C (H) at different potentials varied from 0.5 to 0.2 V.

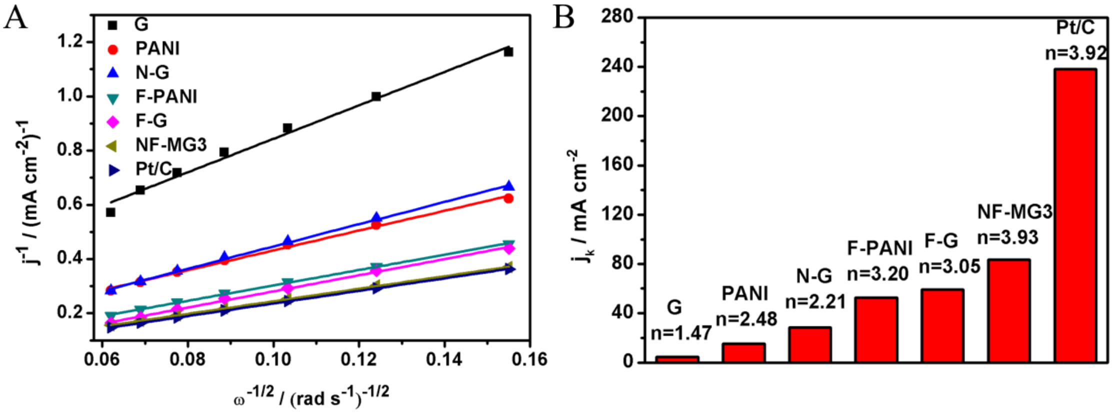

Fig. S8 (A) K-L plots of G, PANI, N-G, F-PANI, F-G and NF-MG3 and Pt/C at 0.4 V. (B) the kinetic current density (j_k) and calculated n at 0.4 V for all samples.

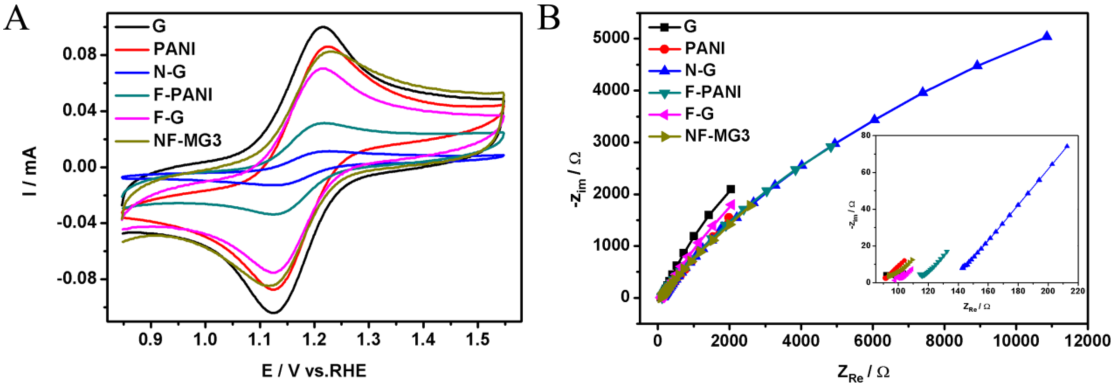

Fig. S9 (A) CV curves and (B) Nyquist plots obtained from EIS of G, PANI, N-G, F-PANI, F-G and NF-MG3 in 0.1 M KCl containing 5 mM $[Fe(CN)6]^{3-/4-}$.

1. Y. G. Li and Y. Y. Wu, *J. Am. Chem. Soc.,* 2009, **131**, 5851-5857.
2. K. J. Mayrhofer, B. B. Blizanac, M. Arenz, V. R. Stamenkovic, P. N. Ross and N. M. Markovic, *J. phys. Chem.. B*, 2005, **109**, 14433-14440.
3. Y. Y. Liang, H. L. Wang, P. Diao, W. Chang, G. S. Hong, Y. G. Li, M. Gong, L. M. Xie, J. G. Zhou, J. Wang, T. Z. Regier, F. Wei and H. J. Dai, *J. Am. Chem. Soc.*, 2012, **134**, 15849-15857.
4. W. Xiong, F. Du, Y. Liu, A. Perez, M. Supp, T. S. Ramakrishnan, L. M. Dai and L. Jiang, *J. Am. Chem. Soc.*, 2010, **132**, 15839-15841.
5. Y. Y. Liang, H. L. Wang, J. G. Zhou, Y. G. Li, J. Wang, T. Regier and H. J. Dai, *J. Am. Chem. Soc.*, 2012, **134**, 3517-3523.
6. X. Sun, Y. Zhang, P. Song, J. Pan, L. Zhuang, W. Xu and W. Xing, *ACS Catalysis*, 2013, **3**, 1726-1729.
7. Y. Y. Liang, Y. G. Li, H. L. Wang, J. G. Zhou, J. Wang, T. Regier and H. J. Dai, *Nat. Mater.*, 2011, **10**, 780-786.
8. L. Chen, B. Wei, X. T. Zhang and C. Li, *Small*, 2013, **9**, 2331-2340.
9. S. Jiang, C. Zhu and S. Dong, *J. Mater. Chem. A*, 2013, **1**, 3593-3599.
10. J. Benson, Q. Xu, P. Wang, Y. Shen, L. Sun, T. Wang, M. Li and P. Papakonstantinou, *ACS Appl. Mater. Interf.*, 2014, **6**, 19726-19736.
11. J. Zhu, C. He, Y. Li, S. Kang and P. K. Shen, *J. Mater. Chem. A*, 2013, **1**, 14700-14705.